



City Research Online

City, University of London Institutional Repository

Citation: Malgarinos, I., Nikolopoulos, N. & Gavaises, M. (2017). Numerical investigation of heavy fuel droplet-particle collisions in the injection zone of a Fluid Catalytic Cracking reactor, part II: 3D simulations. *Fuel Processing Technology*, 156, pp. 43-53. doi: 10.1016/j.fuproc.2016.09.012

This is the accepted version of the paper.

This version of the publication may differ from the final published version.

Permanent repository link: <https://openaccess.city.ac.uk/id/eprint/15679/>

Link to published version: <https://doi.org/10.1016/j.fuproc.2016.09.012>

Copyright: City Research Online aims to make research outputs of City, University of London available to a wider audience. Copyright and Moral Rights remain with the author(s) and/or copyright holders. URLs from City Research Online may be freely distributed and linked to.

Reuse: Copies of full items can be used for personal research or study, educational, or not-for-profit purposes without prior permission or charge. Provided that the authors, title and full bibliographic details are credited, a hyperlink and/or URL is given for the original metadata page and the content is not changed in any way.

City Research Online:

<http://openaccess.city.ac.uk/>

publications@city.ac.uk

Numerical investigation of heavy fuel droplet-particle collisions in the injection zone of a Fluid Catalytic Cracking reactor, Part II: 3D simulations

Ilias Malgarinos^{1*}, Nikolaos Nikolopoulos^{1,2} and Manolis Gavaises¹

1: School of Mathematics, Computer Science & Engineering, City University London, Northampton Square, EC1V 0HB London, UK, *Corresp. Author – e-mail: Ilias.Malgarinos.1@city.ac.uk

2: Centre for Research and Technology Hellas, Chemical Process and Energy Resources Institute, Egialeias 52, Marousi, Athens, Gr-15125, Greece

Abstract

This study investigates the collisions between heavy gasoil droplets and solid catalytic particles taking place at conditions realized in Fluid Catalytic Cracking reactors (FCC). The computational model utilizes the Navier-Stokes equations along with the energy conservation and transport of species equations. The VOF methodology is used in order to track the liquid-gas interphase, coupled with a dynamic local grid refinement technique in order to minimize the computational cost. Phase-change phenomena, as well as catalytic cracking surface reactions (2-lump scheme) are taken into account. In this paper, the numerical model is extended to investigate the droplet-particle collision process in three dimensions. In order to save computational resources, only half of the droplet is investigated, by imposing symmetry conditions. Firstly, single droplet-catalyst collisions are simulated and compared against the corresponding ones provided by 2D axisymmetric simulations and afterwards, the model is applied for the characterization of the collision dynamics between a single droplet and a particle cluster, i.e. a realistic 3D particle configuration. As the droplet flows through the space between the catalytic particles, important phenomena are observed, such as a) drop levitation due to the formed vapour layer and b) a thin liquid sheet formation, both of which affect the rate of gasoline production, as well as predictions for liquid pore blocking mechanism; a phenomenon frequently observed industrially. Results indicate that gasoline production decreases when the collision target is a particle cluster, instead of a single catalyst, as the corresponding contact area decreases.

Keywords: VOF; FCC; droplet; particle; cluster; collisions

Nomenclature

<i>Acronyms</i>			
CFD	Computational Fluid Dynamics	$We = \rho_{liq} u_0^2 D_0 / \sigma$	Weber number (-)
cpR	Cells per Radius	γ	Mass fraction (kg-specie/kg-gas)
DTP	Droplet To Particle size ratio		
FCC	Fluid Catalytic Cracking	Greek letters	
LPG	Liquefied petroleum gas	α	Liquid volume fraction (-)
UDF	User defined Function	θ	contact angle (°)
VOF	Volume of Fluid Method	μ	dynamic viscosity (kg/ms)
		ρ	Density (kg/m ³)
<i>Symbols</i>		σ	surface tension coefficient (N/m)
D	Diameter (m)	τ	Non-dimensional time (= t_{u_0} / D_0)
$Re = \rho_l u_0 D_0 / \mu_l$	Reynolds number (-)		
RR	Reaction rate (kmol/g _{cat} s)	<i>Subscripts</i>	
SSA	Specific Surface Area (m ² /g)	gas	Gas
t	Time (s)	l	Liquid
T	Temperature (K)	o	initial condition
\vec{u} (u,v,w)	Velocity (its components) (m/s)	p	Particle
V	Volume (m ³)		

1. Introduction

The collision of liquid droplets with spherical particles appear in many engineering applications such as particle spray coating, spray drying, as well as inside industrial fluidized bed reactors. An example of the latter, are the FCC (Fluid Catalytic Cracking) reactors, which are an integral part of modern refineries and act as the main focus of the current work. In the FCC reactors, the contact between atomized heavy fuel droplets and solid catalytic particles results in the “cracking” of the long chain heavy petroleum molecules (gasoil) to shorter chain ones (gasoline, LPG), that are industrially more useful.

The “cracking” reactions take place between the vapour produced by the hot evaporating heavy fuel droplets and the catalysts’ surface [1]. These reactions occur throughout the whole length of the reactor. However, as pointed out by [2-4], there is a need to interpret in a better way the phenomena that take place in the injection zone of such reactors, as the “pre-cracking” happening in this region affects product yield selectivity [4], while also, as it is observed industrially, the non-evaporated liquid originating from the injected droplets hitting the particles may end up blocking their pores and thus result in their deactivation [5].

Experimental studies (selective studies include [6-10]) have been used in the past in order to investigate this zone, as well as the whole reactor, however, only general observations are made concerning droplet sizes, temperatures, locations and evaporation, due to the difficulty that lies in liquid spray behaviour characterization in this complex mixing zone. Moreover, in Computational Fluid Dynamics simulations [2, 3, 11-14], the injection zone is investigated from a large-scale perspective, meaning that the level of detail used cannot capture the complex and violent phenomena that happen when cold droplets are injected in the hot injection zone.

Interface tracking methods can provide the advanced level of detail needed for such investigations. In [15-17], the first efforts to involve single droplet dynamics to the FCC industry were recorded, however, to the authors’ best of knowledge, the conditions investigated were never close to the real FCC ones. In Part I of the present study, a first try was reported to simulate single droplet-particle collisions at realistic FCC operating conditions, taking into account both droplet evaporation as well as cracking reactions at micro-scale. In Part I, the numerical framework was presented, followed by a parametric investigation of single droplet-particle collisions on a two-dimensional framework.

In the present paper, that forms the second part of this two-part study, the attention is turned towards the collision between droplets and realistic particle configurations, as that of a particle cluster. After a thorough examination of the available open source literature and to the best of authors’ knowledge,

limited material exist (both experimental and numerical) concerning the investigation of the physical phenomenon of a droplet impacting onto a particle cluster. Only one numerical work was traced that included the deformation of a single droplet resulting by the motion of two particles [18]. In this work, the authors use the Level-Set function in order to track the liquid-gas interface motion, while they use a distributed-Lagrange-multiplier based method in order to account for the presence of particles. Initially, two particles are placed off-centre from each other, while a liquid droplet is placed in between. The particles start moving in opposite direction, which results in the squeezing, deformation and breakup of the liquid droplet. However, the operating conditions of this work fall out of the scope of FCC units.

Based on the scarce material found, this work tries to fill the identified gap and focuses on the phenomenon of droplet impingement onto particle clusters under realistic FCC conditions. The purpose of the present paper is to extend previous 2-D investigation made in Part I to three-dimensions. Model verification against the 2D predictions is performed, since no experimental results can be found. To the best of the author's knowledge, the evaporation of the droplet, as well surface cracking reactions were taken into account for the first time. In the next section, a brief description of the numerical model is initially given. The simulation of single droplet-particle collisions on a 3D framework is then described, followed by the impact of a single droplet on a particle cluster.

2. Numerical Methodology

The CFD numerical model presented in Part I is utilized in order to simulate the cases of interest. The model solves the Navier-Stokes equations for the prediction of fluid flow, along with the energy conservation equation and transport of species equations. The Volume of Fluid Method (VOF) is used for interphase tracking. The equations are solved in the commercial software ANSYS FLUENT [19], where User Defined Functions (UDFs) have been defined for the implementation of a phase change model (based on kinetic theory of gases [20] for gasoil droplet evaporation), surface cracking reaction rate, as well as a dynamic local grid refinement technique. This technique is applied so that the refined region of the grid follows liquid motion dynamically and thus computational cost is decreased compared to a uniform grid having the same resolution at the liquid-gas interphase. A 2-lump scheme represents the catalytic cracking reactions (kinetics taken from [21]), while the material properties of petroleum gasoil and gasoline are represented by those of single species n-pentacosane ($C_{25}H_{52}$) and n-heptane (C_7H_{16}) respectively (Carl L. Yaws properties [22-24]). The "cracking" pathway begins on the gasoil droplet that evaporates in order to form gasoil vapour, which subsequently, in the presence of the catalytic particle surface, reacts to produce gasoline. Surface porosity is taken into account by a Specific Surface Area

(SSA) variable for the catalyst. The extension of the models presented in Part I to three dimensions is straightforward.

3. Results and Discussion

3.1 Cases Examined

Firstly, the three-dimensional numerical model is verified against the results of the 2D single-droplet particle collisions presented in Part I; then it is utilized to investigate the droplet collision with a particle cluster. The comparison of the current cases with the 2D axisymmetric results is dictated by the lack of similar works in literature, while additionally, it offers a way to evaluate the efficiency of the 3D model and probably spot any effects of three dimensional flow details on the evolution of the phenomenon. The enumeration of the cases is in correspondence to the ones having the same operating conditions in Part I, using the multiplication symbol (example, Case2, Case2*). The three cases selected to serve for this verification are presented in Table 1; they represent two cases of DTP=1, where the effect of impact velocity is examined (Case2* to Case4*, 15m/s to 30m/s) and one of DTP=2 for the evaluation of droplet to particle effect on the phenomenon evolution. Cases2* and 7* represent the best/worst case scenario in terms of gasoline yield production, based on the results presented in Part I of this paper.

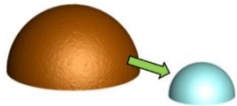
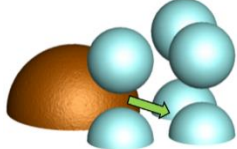
Case No.	DTP	U_o	T_p	We	Re	Refinement Levels	
<u>3-D Single droplet-particle collision</u>							
2*	1	15	1000	4266	2272	3	
4*	1	30	1000	17062	4544	3	
7*	2	30	800	34124	9088	2	
<u>3-D Single droplet-particle cluster collision</u>							
9	2	30	1000	34124	9088	2	

Table 1. Cases investigated for droplet-particle/particle cluster collisions in FCC reactor injection zone.

The last case “droplet-impact-onto-a-cluster” can only be simulated in three-dimensions, as there is no symmetry axis. For this phenomenon, only one cluster formation scenario is simulated; the operating conditions of this scenario correspond to a realistic/representative collision situation which can be found in FCC reactors. As catalyst to oil ratio is high (Part I), a droplet is expected to collide with many

particles along its motion. Moreover the chosen size of the droplet and its impact velocity are closer to the typical current FCC values (Part I). The operating conditions of the runs are presented in Table 1, while in Table 2, the common properties used in all runs are given. It is worth pointing out that all operating conditions resemble those exhibited in the injection zone of FCC reactors [1, 25]. Three dimensional simulations offer the possibility to simulate every possible collision scenario (including off-centre) and therefore lift the restriction of head-on collisions implicated by the 2D-axisymmetric simulations presented in Part I.

P_{oper} (Pa)	T_{drop} (K)	T_{gas} (K)	D_p (μm)	Θ ($^\circ$)
202,650	550	800	75	100

Table 2. Operating conditions for all cases.

3.2 Computational domain and Boundary conditions

The computational domains which were used for the three-dimensional cases presented above are depicted in Figure 1 for the case of single droplet-particle collision (cases 2*,4*,7*) and Figure 2 for the droplet-particle cluster collision (case 9). Half of the droplet is simulated in all cases (a domain of 180°). For cases 2* and 4*, the total dimensions of the domain at the direction of droplet motion (X-axis) and at transverse direction (Y-axis) are similar to the two-dimensional domain, shown as a grid slice in Figure 1a,b.

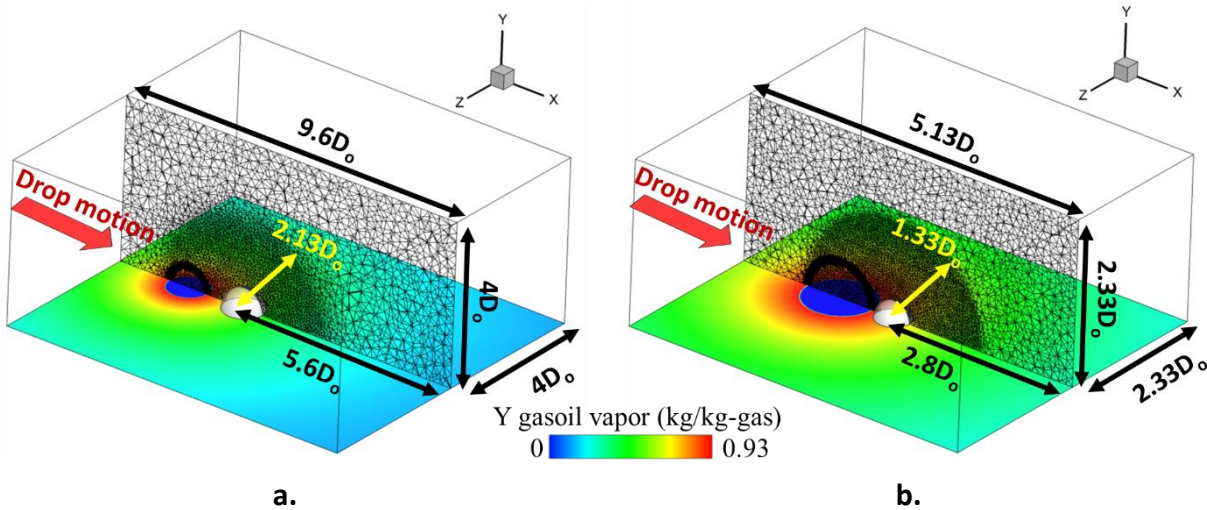


Figure 1. Computational domain used for Cases a) 2* and b) 4*. Bottom plane coloured by gasoil vapour initial mass fraction.

The third dimension, added in the 2D domain resembling the depth, takes the same value with the vertical one. For case 7*, the total dimensions of the domain were much smaller than in the corresponding 2D case. The initial gasoil vapour mass fraction is coloured at the bottom plane of the computational domains and is presented in Figure 1, while resembles the 2D simulations.

In Figure 2, the numerical domain applied for case 9 is presented. The initialized liquid droplet is depicted in dark orange colour, while the particles are coloured grey. The domain dimensions are smaller compared to the domains presented in Figure 1; however this choice was mandated by the high amount of computational cost required in order to solve this problem within a reasonable timeframe. Figure 2 presents the top view of the particle cluster arrangement. Three particles are in the same plane with the droplet half-symmetry plane, while the location of the 3 remaining particles is the same as the others, however with an offset in the Y-axis direction. For easier readability of graphs that follow, the lower level particles, placed in the same plane as the droplet, will be named as A_i , B_i and C_i , while the higher level ones will be referred to as A_h , B_h and C_h . The particle name notation is depicted in Figure 2b. From top view, as the droplet impacts the catalyst particle cluster arrangement, A and B are the names of the side particles the droplet encounters on its way, while the C name is given to the centre particle, which lies in the direction of droplet motion.

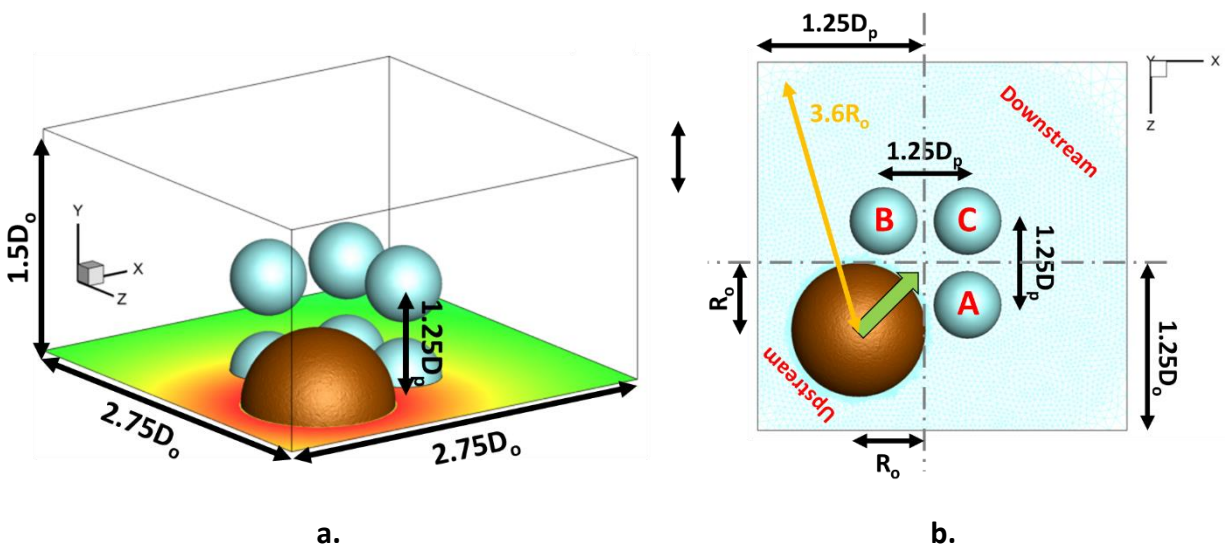


Figure 2. a) Computational domain used for the simulation of Case 9. b) Particle cluster arrangement and notation used.

The boundary conditions applied in all domains were pressure inlet (zero first gradient for all variables, pressure fixed value 202,650 Pa) for all boundaries, except the symmetry boundary cutting the droplet in half and the hemi-spherical surface which was set as a wall; a fixed contact angle given in Table 2 was assumed.

The applied numerical grids comprised of tetrahedron cells. The size of the smallest cell in the domain was set equal to the corresponding of the 2D case, while keeping the same cell width (5.89 μm), to allow for the comparability of the 2D and 3D predictions. Thus, the catalyst particle surface was split in accordance to the 2D axisymmetric case (40 divisions along the symmetry axis). Further away from the particle surface, a spherical zone was used with the same cell dimensions (slice of grid presented in Figure 1a,b and Figure 2b); beyond this zone, the cell width was set to approximately 20 μm . The droplet was initially placed at a one droplet diameter distance away from the particle impact point for cases 2*, 4* and at a distance of $D_0/5$ for case 7*. In case 9, the initial droplet distance is shown in Figure 2b. The droplet radius was covered by 51 cells in all cases (51 cpR).

Table 3 presents significant information concerning the grid size and time that is required for the calculation of all cases. Moreover, the number of cells that a uniform grid would need in order to simulate the same phenomenon achieving the same grid resolution at the droplet interface is presented. It is obvious that the local refinement algorithm, decreases a lot the computational cost of the cases, as a case of uniform dense grid of 73.6M cells would possibly run only at a supercomputer station. The most computationally expensive runs are the high impact velocity cases 4* and 9, as the large velocity values induced in the domain, both at the liquid sheet tip, as well as the particle surface (at the vapour layer), lead to reduction of the time-step. In the last case, the 6 particles in the domain make the numerical problem more complex, as the induced velocity field reduces the time-step from the moment of impact till the end of the simulation.

Cases	Coarse grid (mill cells)	Initial grid (mill cells)	Maximum grid (mill cells)	Processors	Time to simulate $\tau=1.5$ (in days)	Uniform equiv. grid (mill cells)
2*	0.51	1.84	7.92	36	18	32.1
4*	0.51	1.84	7.94	36	54	32.1
7*	0.93	2.29	4.05	36	19	14.9
9	1.15	2.2	4.85	36	89	73.6

Table 3. Number of cells and simulation time for runs performed (for the sake of comparison the time elapsed is the number of days it took to reach a runtime of $\tau=1.5$).

3.3 Results

In the following section, all results are presented in non-dimensional form, so that the comparison among all cases is direct and general conclusions can be drawn. Non-dimensional time $\tau (=tu_oD_o)$ is set to zero at the time instant of impact.

3.3.1 Single Droplet-Particle collisions

3.3.1.1 *DTP=1, effect of impact velocity*

In Figure 3, the temporal evolution of drop deformation throughout the process of its collision with the catalytic particle is presented both for cases 2* (3D) and 2 (the corresponding 2D one). In this figure, the contours of gasoline mass fraction in gas phase are presented, while in the three-dimensional results, the iso-surface of $\alpha=0.5$ is also shown.

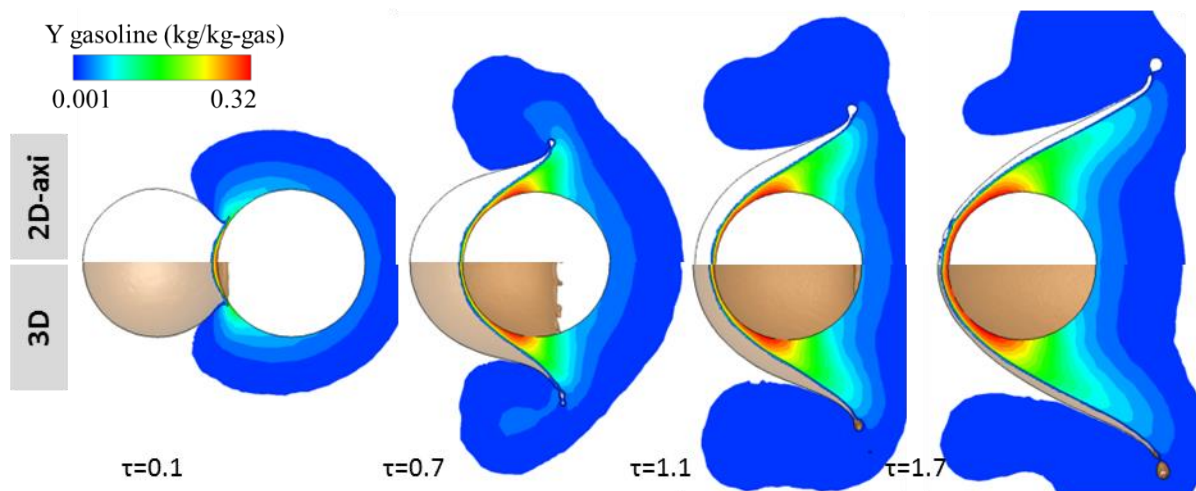


Figure 3. Effect of CFD simulation dimensions on collision outcome for a $DTP=1$, $U_o=15\text{m/s}$, $T_p=1,000\text{K}$ impact, Case2 (top), Case2* (bottom). Contour of the produced gasoline mass fraction (kg-gasoline/kg-gas). The iso-surface of $\alpha=0.5$ is depicted for the 3D case (bottom).

Results indicate that the droplet shape, as well as gasoline mass fraction distribution throughout the phenomenon are similar in both the 2D and the 3D cases. The droplet deforms into a thin liquid sheet that, moves away from the catalyst surface, as spreading along it. At $\tau=0.7$, the formation of fingers is observed in the three-dimensional case. These finger structures, as well as subsequent liquid sheet break-up are shown in 3D view in Figure 4, during the final stages of the phenomenon. The expanding liquid sheet reaches its maximum deformation (elongation both along the X-axis and YZ plane) at

approximately $\tau=2.1$, at a time instant it starts breaking-up on the impact side, probably due to high catalyst temperature that promotes higher evaporation rate. The break-up mechanism travels along the whole liquid expanding structure (lamella) up to time $\tau=2.9$. During these time instants, the liquid form disintegrates violently in the form of a large number of secondary droplets. The liquid form taken in this Figure resembles the “splash with ligaments” regime presented in the work of [26] for droplet impingement on a heated flat surface. On top of Figure 4 results from the corresponding 2D-axisymmetric simulations presented in Part I are depicted. As it is obvious that 2D simulation cannot actually represent the evolution of ligament break-up into satellite droplets. such axisymmetric results cannot be trusted for non-dimensional time higher than $\tau=2$.

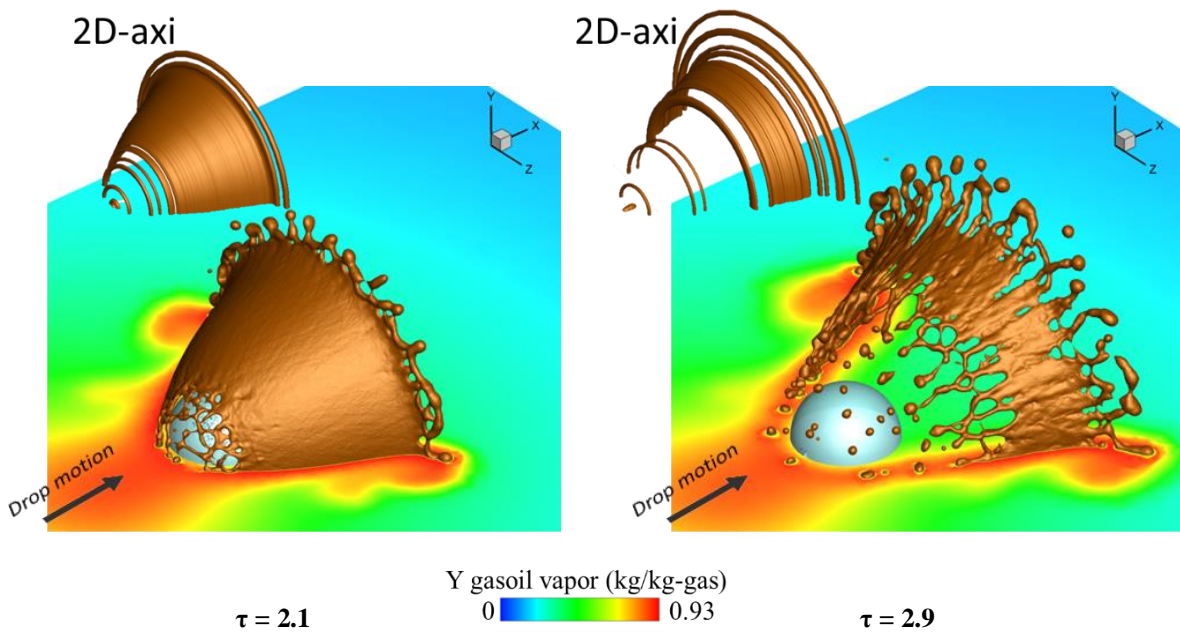


Figure 4. Formation of finger structures ($\tau=2.1$) and sudden break-up ($\tau=2.9$) are predicted in Case 2* (3D). Gasoil vapour mass fraction (kg-gasoil/kg-gas) is depicted on the symmetry boundary. Corresponding images from the revolution of 2D-axi results for 3D representation are added on top of the figure.

Overall, the 3D numerical model behaves robustly, compared to the 2D axisymmetric results. Finger structure formation and subsequent sheet break-up are three-dimensional phenomena that start at approximately $\tau=2$ and cannot be captured by the 2D simulations.

The same conclusions can be drawn for cases 4 and 4* presented in Figure 5, following the similar droplet shapes and gasoline production levels for the 2D and 3D approaches. The perturbations observed on the inner (particle) side of the liquid sheet at $\tau=0.1$ and $\tau=1.1$ in the axisymmetric case are not observed in the three dimensional one, as the predicted drop shape seems to be smoother. The

formation of thinner finger structures is also predicted, a phenomenon which cannot be captured in 2D simulations.

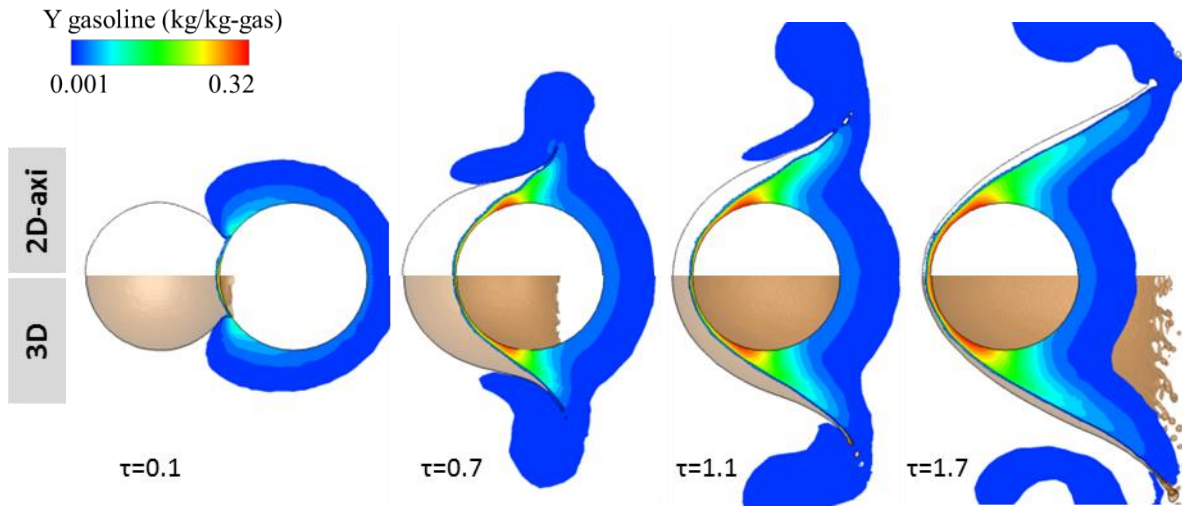


Figure 5. Effect of CFD simulation dimensions on collision outcome for a $DTP=1$, $U_0=30\text{m/s}$, $T_p=1,000\text{K}$ impact, case4 (top), case4* (bottom). Contour of the produced gasoline mass fraction (kg-gasoline/kg-gas). The iso-surface of $\alpha=0.5$ is depicted for the 3D case (bottom).

A vapour layer is formed between the droplet and the particle surface that keeps the droplets away from touching the catalyst. The comparison of the vapour layer thickness as predicted for the 2D and 3D simulations is presented in Figure 6.

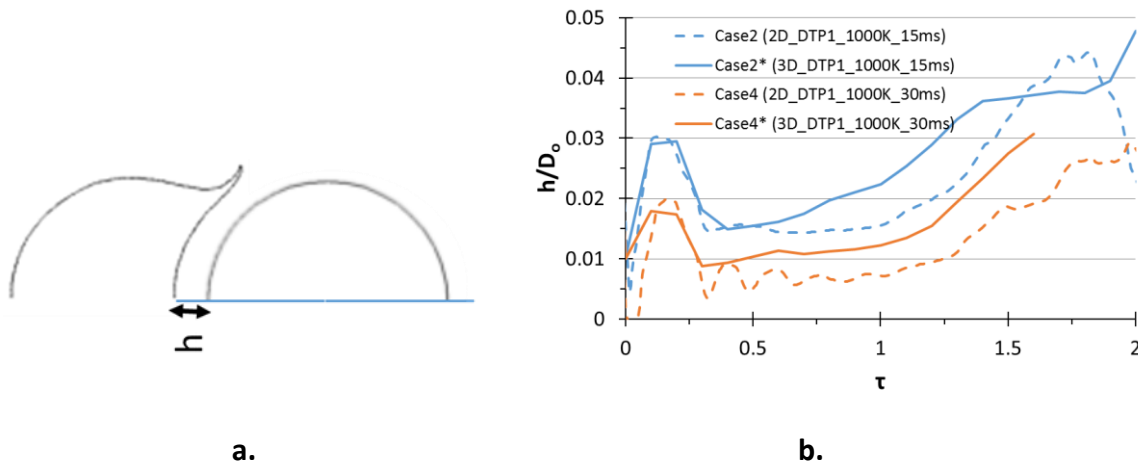


Figure 6. a) Definition of the vapour layer thickness at the impact point, b) Temporal evolution of the vapour layer thickness at the impact point for cases 2,2*,4,4*.

A slightly thicker vapour cushion is predicted in the three-dimensional domains for both the low/high impact velocity cases, especially for dimensionless times higher than $\tau=0.5$. For the latter case (case4*), a smoother transition in vapour thickness values for $0.25 < \tau < 0.75$ is predicted for the three-dimensional run, when compared to the 2D one. Overall, results indicate that there is both qualitative and quantitative agreement between 2D and 3D simulations.

Similar conclusions are drawn from observing gasoil conversion (gasoline production) levels, as well as surface cracking reaction rate throughout the phenomenon, as shown in Figure 7. The 2D cases seem to over predict slightly the reaction rate and products. Once again, the three-dimensional results are smoother for case 4* compared to 4.

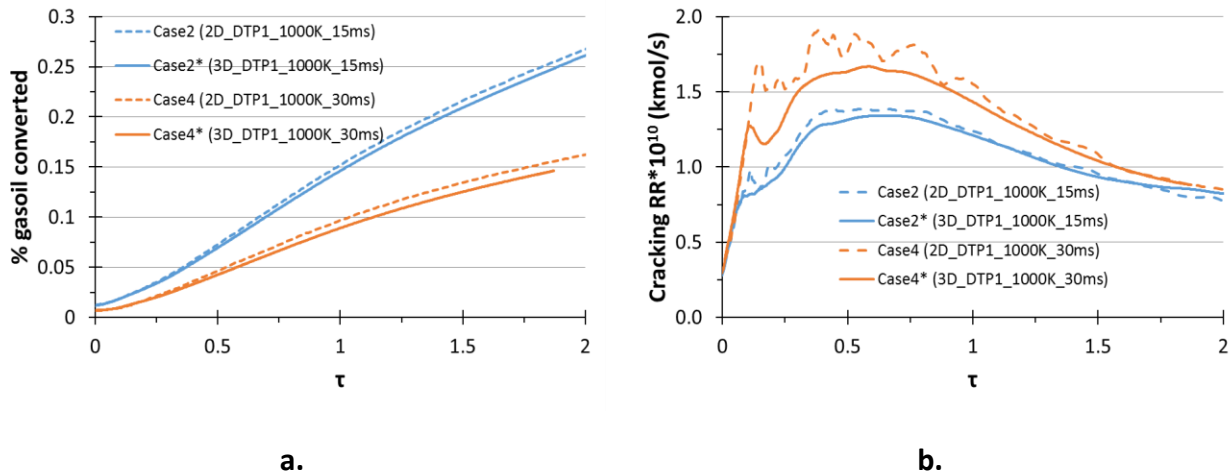


Figure 7. a) Percentage of gasoil converted to gasoline yield (kg-gasoline/kg-liq %) and b) cracking reaction rate, both plotted against non-dimensional time for Cases 2,2*,4,4*.

Finally, similar results between 2D and 3D cases were also obtained for all important parameters such as droplet mean temperature, mean velocity and surface area. Therefore, it can be deduced that the 3D model is robust for DTP=1 cases, while certain three-dimensional phenomena such as finger structures and liquid sheet break-up can be captured. For $\tau \leq 2$, before the appearance of these phenomena, the axisymmetric simulations can be trusted.

3.3.1.2 DTP=2, uncertainty for accuracy in 2d domains

In Figure 8, the temporal evolution of droplet shapes is presented for cases 7* (3D) and 7 (2D), along with the produced gasoline mass fraction. For this case, the results between 2D and 3D domains change

significantly. In the 2D domain, it is observed that the droplet is sucked in ($\tau=0.5$) by the wake vortex ring formed downstream the impacted solid particle. Subsequently, the expanding liquid sheet coalesces at the symmetry axis ($\tau=1$) and progresses forward. On the contrary, in the 3D case, it is again observed that the liquid sheet is sucked in by the wake vortex ring, however, much later during the collision process ($\tau=1.4$). The liquid sheet forms a closed surface, which is hollow inside.

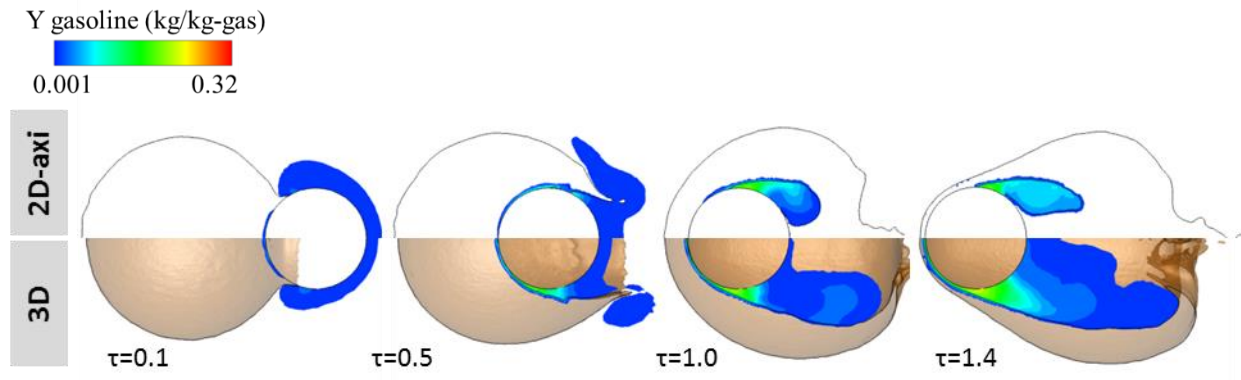


Figure 8. Effect of CFD simulation dimensions on collision outcome for a $DTP=2$, $U_o=30\text{m/s}$, $T_p=800\text{K}$ impact, case7 (top), case7* (bottom). Contour of the produced gasoline mass fraction (kg-gasoline/kg-gas). The iso-surface of $\alpha=0.5$ is depicted for the 3D case (bottom).

For these specific conditions an “igloo” shaped form is presented in a close up view in Figure 9. At $\tau=0.66$, the “igloo” shape starts to form, which afterwards moves downstream from the impact side and accumulates to a liquid mass which resembles a shape similar to the initial one (“copy” droplet), but with its core to be empty of liquid (hollow).

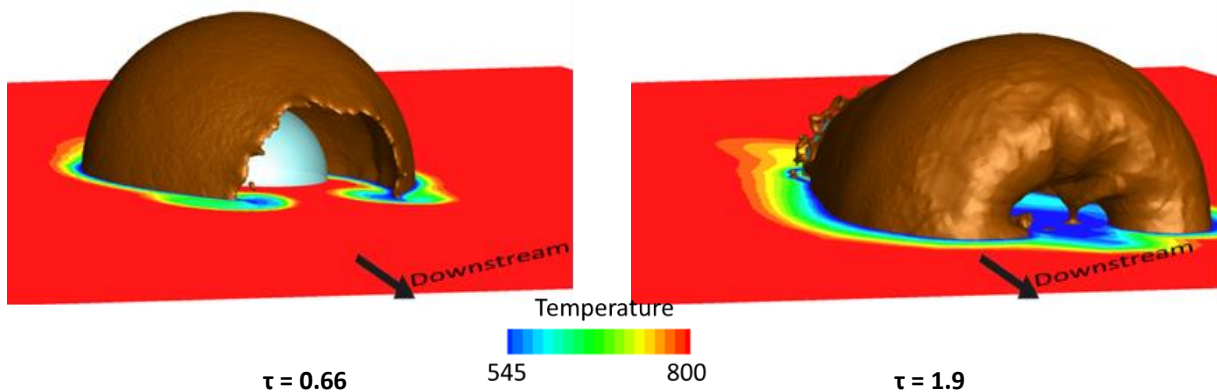


Figure 9. Igloo shaped form ($\tau=0.66$) and “copy” droplet ($\tau=1.9$) are predicted in the 3D case7*. Temperature contour (K) is depicted on the symmetry boundary.

This large difference between the 2D and 3D simulation on this case can be attributed to the different predicted liquid-solid contact, quantified in terms of vapour layer thickness, and presented in Figure 10. As the droplet moves along the particle surface, a very thin vapour layer is formed in the 3D domain, while for the 2D domain, the drop comes in direct contact with the solid surface throughout the whole phenomenon ($h \sim 0$). This higher contact between solid-liquid does not allow the formed liquid sheet to move away from the surface, and thus it is sucked in the wake region sooner than what is predicted in three dimensions.

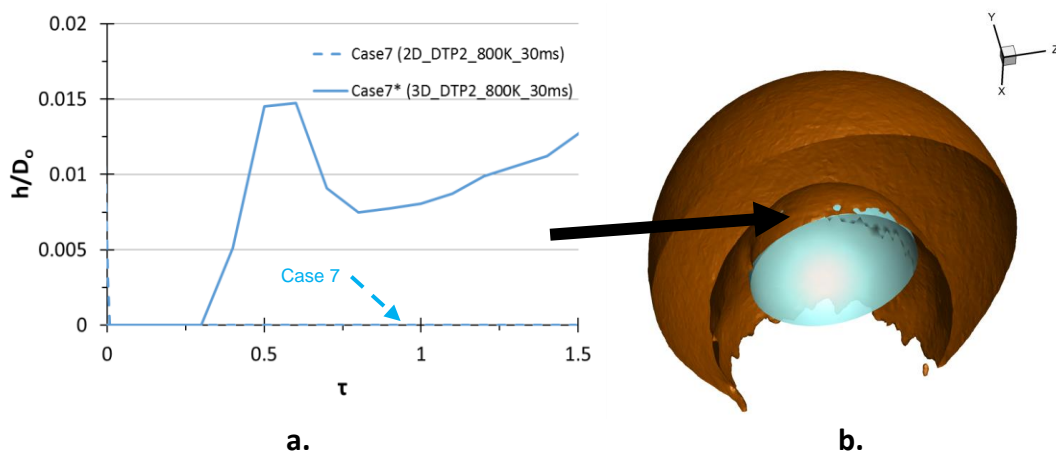


Figure 10. a) Vapour layer thickness temporal evolution for Cases 7, 7*, b) Solid particle partial wetting at $\tau=0.66$ is predicted in the 3D case.

However, this change is of utmost importance to the progression of the phenomenon and affects the conversion of gasoil, i.e. production of gasoline. As it seems from Figure 11, the formation of gasoline in the 3D case precedes the 2D one in time, as the vapour layer formed at approximately $\tau=0.4$ (Figure 10) promotes cracking reactions and thus gasoline formation. On the other hand, the reaction rate in the 2D case is higher than in the 3D one, probably due to the fact that gasoline is also produced at the wake side of the droplet.

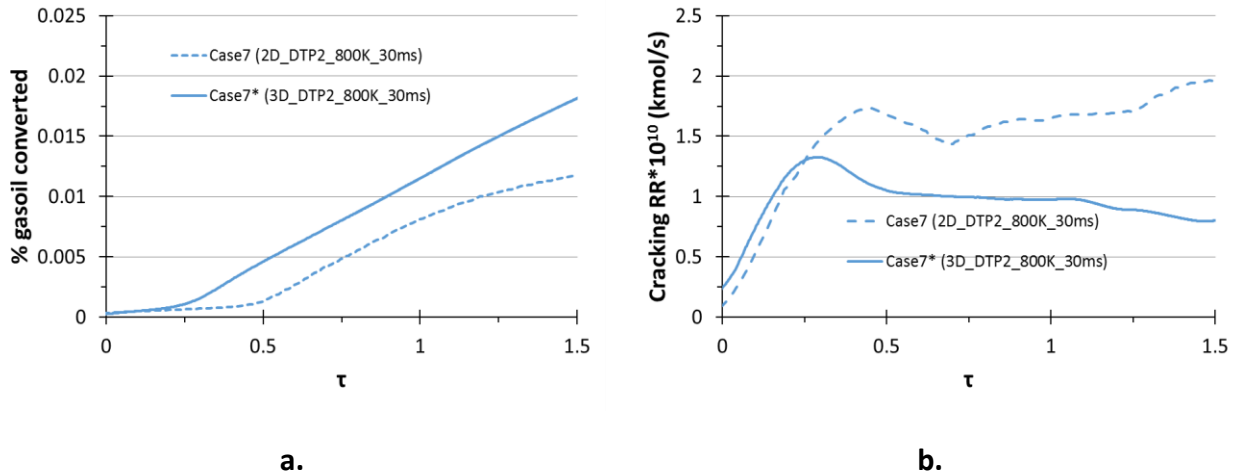


Figure 11. a) Percentage of gasoil converted to gasoline yield (kg-gasoline/kg-liq %) and b) cracking reaction rate, both plotted against non-dimensional time for cases 7,7*.

Overall, in collisions where increased solid-liquid contact is expected, as in the case presented in this section, 2D axisymmetric simulations seem to fail in representing correctly the physical phenomena predicted by the 3D model, especially the levitation of the droplet, followed by the subsequent production of gasoline. This is a very interesting observation, as the worst case scenario type cases will have to be simulated using 3D domains. In DTP=1 cases, where low solid-liquid contact is expected, results between 2D and 3D simulations are closer.

3.3.2 *Particle cluster collisions*

In Figure 12, the temporal evolution of droplet shape after its impingement onto the particle cluster arrangement is presented, as viewed from a downstream position. On the top set of pictures, the drop-gas interface is presented, plotted with the use of the iso-surface of $\alpha=0.5$, while on the bottom part of the figure, a volume representation of the produced gasoline lump specie is shown, coloured by gasoline (n-heptane) mass fraction in the gas mixture. Time is non-dimensionalised, taking as impact reference point, i.e. $t=0$, the time instant when the droplet first touches one of the spherical catalyst particles. As the droplet moves in between the space left from the presence of the solid particles, it starts to deform into a liquid sheet ($\tau=0.2$) as observed in single droplet-particle collisions.

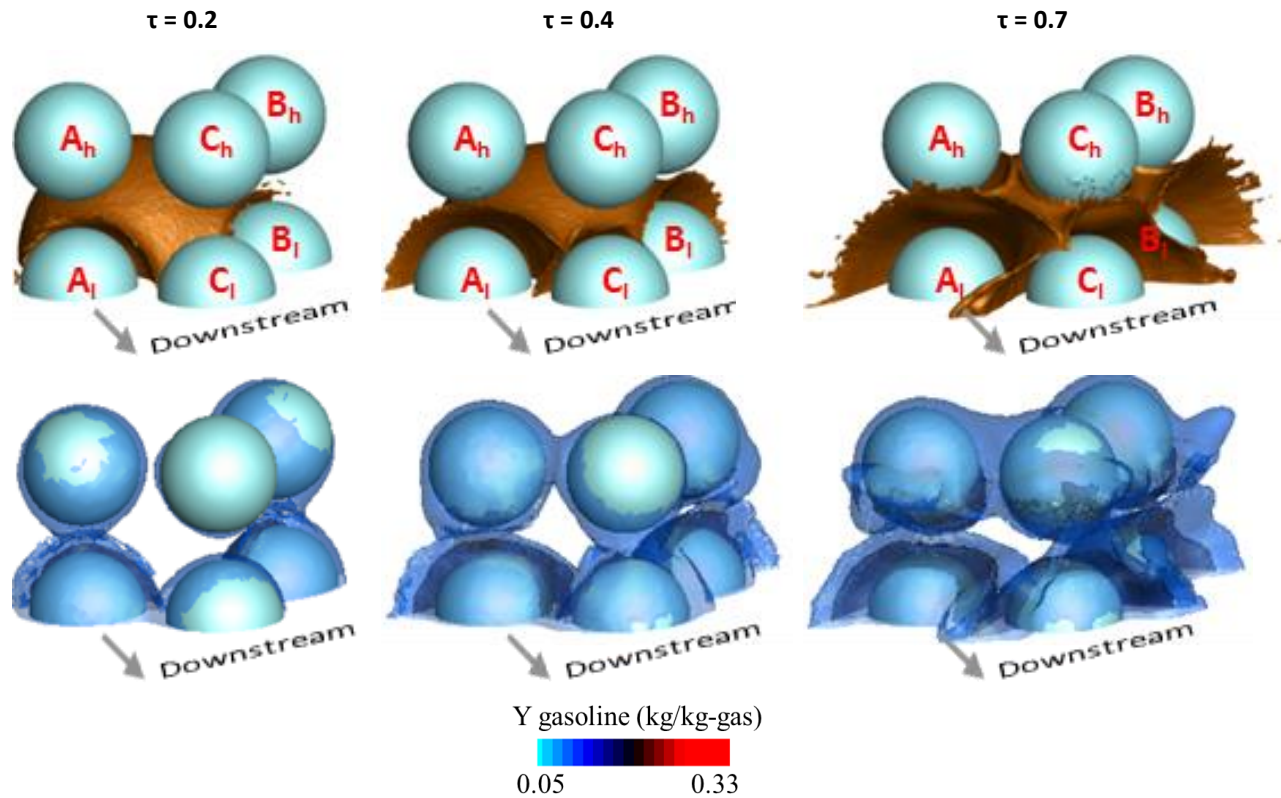


Figure 12. Drop impact onto a particle cluster. Top row shows iso-surface of $\alpha=0.5$, bottom row shows gasoline mass fraction volume rendering.

A vapour layer is again formed between the deforming liquid and the catalyst surface. Due to the presence of the high temperature catalysts, the approaching droplet evaporates at a high rate, producing gasoil vapour that subsequently reacts with the catalyst surface and cracks to gasoline. This formed vapour layer poses a barrier to droplet direct contact with the catalyst surface. This phenomenon is promoted due to catalyst high temperature levels (1000K), in contrast to lower ones (as in Case7*), where the liquid can come in direct contact with the solid particle and it is spreading onto that. The first stages of drop levitation on the surface of side particles A_l and B_l is presented in Figure 13 for $\tau=0.05$, where it is obvious that the drop only partially wets the solid surface.

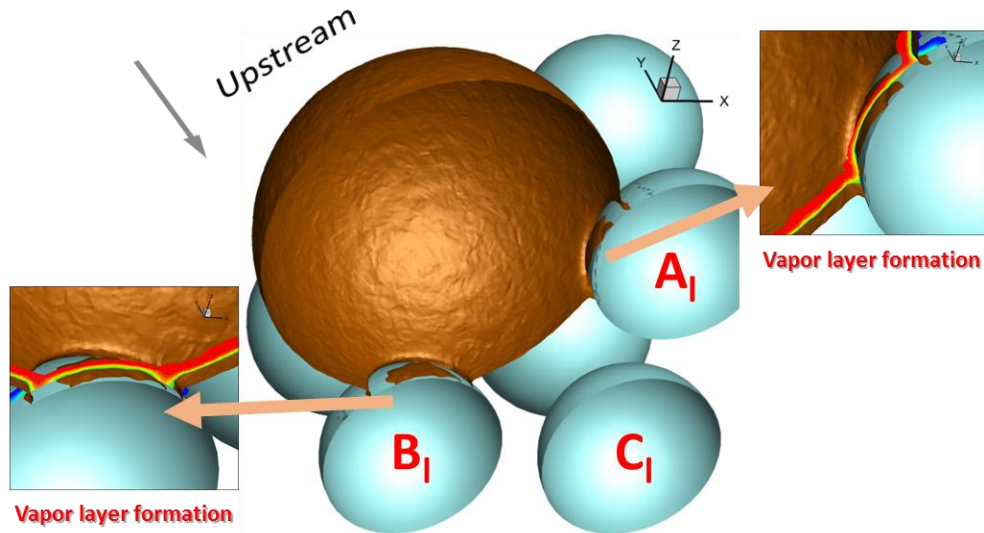


Figure 13. Vapour layer levitating droplet on top of particles ($\tau=0.05$). Two slices of volume fraction field at the proximity of spherical particles are shown, where $\alpha=0.001-0.999$.

As the deformed liquid mass continues its motion across the gap among the particles, liquid sheets are formed close to each particle surface ($\tau=0.4$), as they repel the liquid. This results in complex liquid forms presented in Figure 12, $\tau=0.7$. As the phenomenon progresses and the expanding liquid sheet moves away from the side particles and approaches the central one (C_i), it becomes clear that the flow induced by the presence of this centre particle dominates the evolution of the phenomenon. This is observed in Figure 12, at $\tau=0.7$, as the liquid sheet repels by the centre catalyst; thus leading the droplet to move towards the direction of the other two particles.

The gasoline lump formed follows the shape of the formed liquid sheet. At $\tau=0.2$, gasoline production is increased right after the particle impact, and is high at the point of impact. As the droplet moves inside the particle cluster, one by one the particles are turned on (in the sense of gasoline production) by the presence of gasoil lump gas specie, and the mass fraction of gasoline locally increases. At $\tau=0.4$, the formed gasoline covers almost the whole particle surfaces, with the only exception the top level center particle. High levels of gasoline lump mass fraction are observed close to the impact point, and along the inner side of the formed liquid sheet. At $\tau=0.7$, the high values of gasoline concentration are kept close to the liquid sheet.

For longer times of the process, the formed liquid sheet breaks-up into smaller satellite droplets as presented in Figure 14, $\tau=1.05$. At this point, the droplet merely touches any solid surface, due to its levitation in respect to hot catalysts, as mentioned before. The droplet break-up, is attributed to flow instabilities and possibly, from a numerical point of view, not adequate liquid interface grid resolution.

The prediction of sheet breakup exact time and place falls out of the scope of the current study. In the present paper, a qualitative prediction of drop breakup global locations can be claimed.



Figure 14. Drop break-up after impact on a particle cluster at $\tau=1.05$.

It appears that the most probable locations for liquid sheet breakup are the left and right bounds of the induced liquid shape. At these locations, the liquid sheet is thinner and easier to breakup, while the sheets surrounding the centre particle are thicker. At $\tau=1.05$ the central parts of the liquid sheet form a torus-like shape, which breaks up from the main liquid body. The break-up mechanism can be either driven by Rayleigh type instabilities, starting from either a torus-like or a finger shape, or due to the presence of surface tension, as also explained in [27].

The grid high resolution at the region close to the liquid interface is presented in Figure 15a. Two slices of the domain are depicted, a) the one being the symmetry axis and the other b) a plane ranging 2 degrees from the XZ diagonal. A close up view at the refined cell region is presented in Figure 15b. The length of this region, along the normal direction of the interface, as observed, is kept as small as possible, so that the computational cost for this case can be the minimum possible.

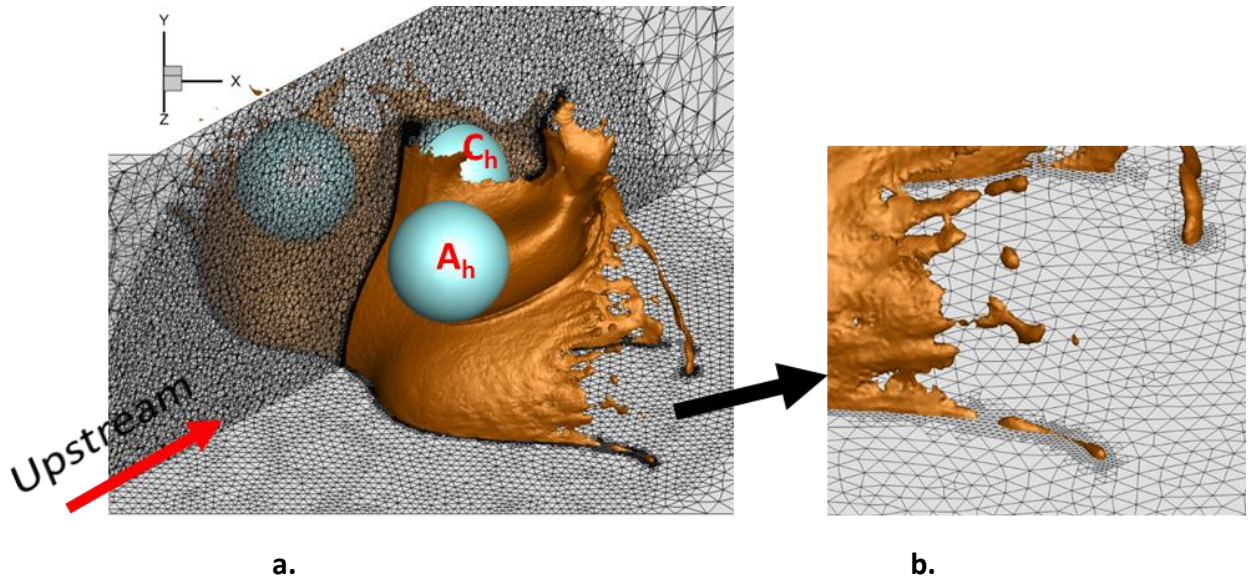


Figure 15. Local refinement algorithm application in the case of drop-particle cluster simulation case. a) Global view, b) Close-up view.

In Figure 16, the temporal evolution of the phenomenon is presented viewed from the upstream direction, where the droplet iso-surface ($\alpha=0.5$) is coloured by the dimensionless velocity magnitude.

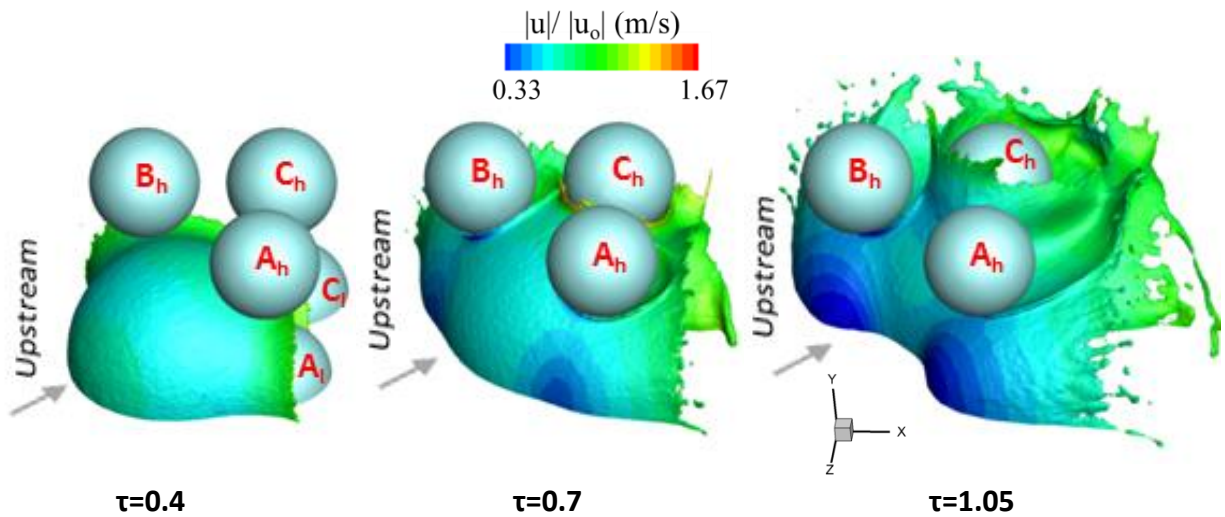


Figure 16. Temporal evolution of drop-particle cluster collision. Droplet is represented by the $\alpha=0.5$ iso-surface coloured by velocity magnitude.

It is clear that at all time instances, the velocity magnitude is higher at the endpoint of the formed liquid mass. The liquid sheet is accelerated by the induced downstream the impact region fluid flow. Velocity values range in-between $1/3$ and $5/3$ of the impact velocity. These high velocity liquid jets break-up at

some point, and then evaporate quicker as the interfacial area of liquid increases dramatically. In FCC reactors droplet break-up is desirable as it promotes quick evaporation and less solid-liquid contact which may result in catalyst pore blocking [5].

In Figure 17 the induced recirculation zones in the area of the impact wake region are shown for droplet impact on a single particle, as well as onto a particle cluster. It is obvious that the recirculation zones induced behind the center particle are similar to the single drop-particle interactions. The side recirculation zones are rotated in a vertical direction. This is probably attributed to the center liquid sheet, which is pushed towards the sides and restricts the fluid flow in the wake region of the side particles to develop naturally. Therefore, this liquid motion induces a change in recirculation zones direction.

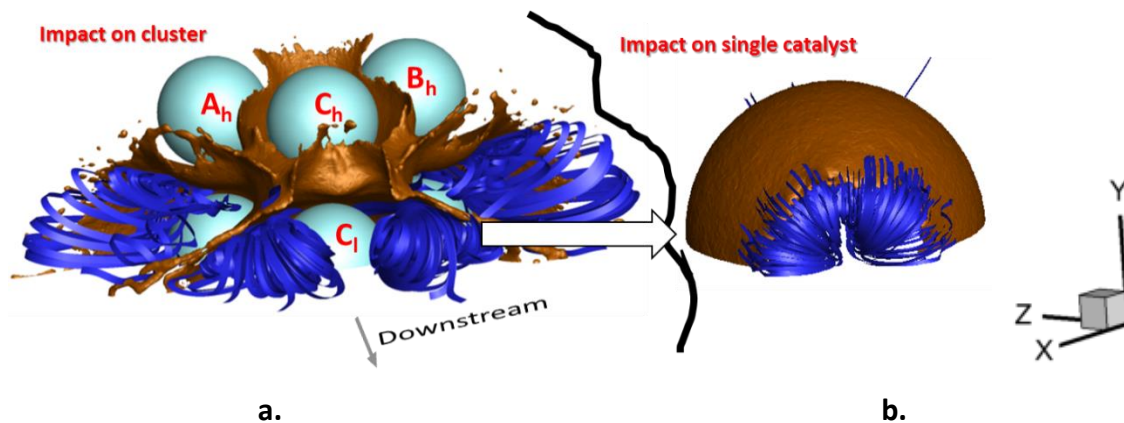


Figure 17. Recirculation zones induced by fluid flow at a) $\tau=1.05$ for droplet impact onto a particle cluster, b) $\tau=0.66$ for droplet impact onto a single particle.

In Figure 18 the gasoline production and total reaction rates for droplet impact onto a single particle (case 9), as well as onto a particle cluster are plotted against the non-dimensional time of the phenomenon. The values are non-dimensionalised by the number of particles that the droplet comes in contact with (1 and 9 respectively). It is predicted that the reaction rate as well as the gasoline production decreases when the droplet hits a particle cluster. The surface area that is in fact used for the production of gasoline in the present case is limited corresponding to nine single droplet-catalyst impacts.

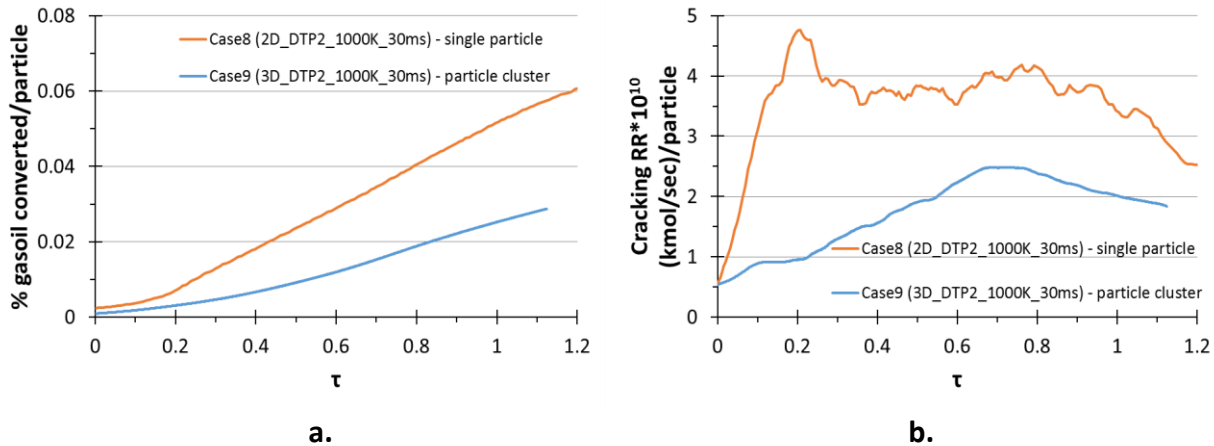


Figure 18. a) Percentage of gasoil converted to gasoline yield (kg-gasoline/kg-liq %) and b) cracking reaction rate, both plotted against non-dimensional time for Cases 8 and 9.

In Figure 19, the droplet average temperature, as well as the non-dimensional drop mass are plotted against the non-dimensional time throughout the whole phenomenon for single droplet-catalyst collisions compared to droplet-cluster collisions. In the latter case, droplet temperature increases in time, in contrast to the general observations made for 2-D single droplet-particle collisions. The presence of nine particles in the cluster contribute to the local increase in gas temperature that results in the increase of heat convection towards the droplet mass.

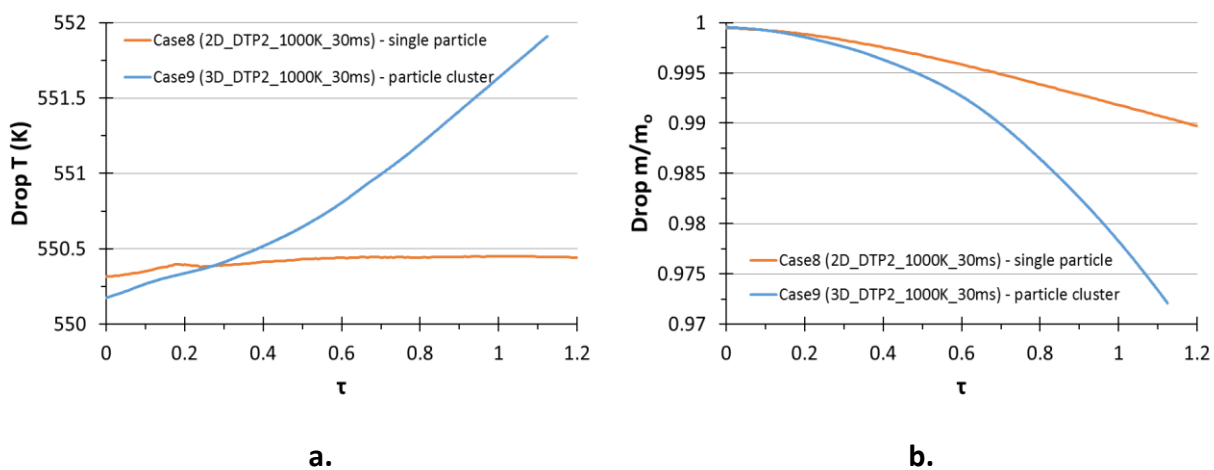


Figure 19. a) Droplet mean temperature and b) Non-dimensional mass, both plotted against non-dimensional time.

Droplet endures a significant evaporation of its mass as it passes through the cluster of particles. However, when compared with the single drop case, the associated mass loss is increased only by 2%

compared to the case of droplet impingement onto one catalyst particle for the same dimensionless period, which means that the particle cluster does not affect significantly the evaporation process and therefore the total mass loss of the droplet.

An interesting observation is made when investigating the particle surface coverage, which is presented in Figure 20. In this Figure, the percent of total particle area which is covered by liquid is plotted against the non-dimensional time for Case9. This is calculated as:

$$\frac{A_w}{A_p} = \frac{\left[\sum_{wall-f} \alpha A_f \right]_{(f \rightarrow \alpha > 0.5)}}{\sum_{wall-f} A_f} \quad (1)$$

From this figure, it is observed that the wetting of particles concerns only a very small percent of its area (up to 1.5%), where the liquid pore blocking mechanism is expected to happen. Moreover, as the droplet impacts all particles, one by one, a spike appears in this graph, where the droplet initially wets partially the particle surface up to the point that it is levitated by the formed vapor layer.

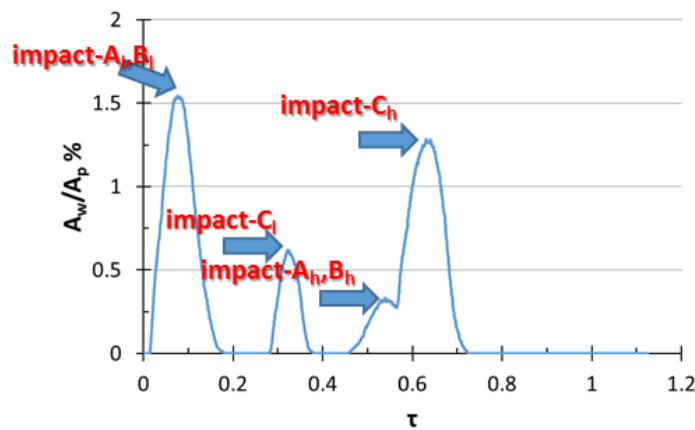


Figure 20. Temporal evolution of the percentage of particles' area which is wetted.

4. Conclusions

In this 2 part study, the Navier-Stokes equations, along with the energy conservation, transport of species equations and the Volume of Fluid two phase flow methodology are used for the investigation of droplet-particle collisions at conditions relevant to those realised in the injection zone of Fluid Catalytic Cracking (FCC) reactors. In the present paper (Part II), the three-dimensional numerical model was verified using the 2D results of Part I. More specifically, 3 cases with DTP=1 and 2 were tested, which included the best/worst case scenarios in respect to gasoline yield. It was shown that the numerical

model behaves robustly and gives similar results between 2D-axisymmetric and 3D domains for the cases where decreased solid-liquid contact is expected (DTP=1 and best case scenario). On the other hand, for the worst case scenario (DTP=2, cold catalyst, high impact velocity), which represents typical FCC droplet/particle sizes, was not reproduced exactly compared to the 2D results. It is concluded that 3D simulations are needed in order to simulate these types of collisions, however this requires further investigation. Afterwards, the numerical model was utilized for the prediction of a droplet impinging onto a particle cluster formation. Results indicate that droplet lifetime does not change significantly in relation to the single drop-particle collision case; however its breakup into more secondary droplets promotes a quicker evaporation time after the collision. It was found that the impingement of a gasoil droplet onto a particle cluster, instead on a single particle decreases catalytic cracking reaction yields as the corresponding contact area decreases. Overall the numerical model behaves in a robust way. Further solid shaped geometrical configurations and their effect on the phenomenon evolution can be simulated with the proposed methodology, which considers as well the existence of complicated non-isothermal conditions.

5. Acknowledgements

The present work was funded by the Marie Curie Fellowship (FP7-PEOPLE-2012-IEF) with Grant Agreement number 329500 funded by the European Commission entitled as “NonFlatImpingement—Droplet Impingement on Non-flat Surfaces”.

6. REFERENCES

1. Ancheyta, J., *Modeling and Simulation of Catalytic Reactors for Petroleum Refining* 2011: Wiley.
2. Theologos, K.N., A.I. Lygeros, and N.C. Markatos, *Feedstock atomization effects on FCC riser reactors selectivity*. Chemical Engineering Science, 1999. **54**(22): p. 5617-5625.
3. Nayak, S.V., S.L. Joshi, and V.V. Ranade, *Modeling of vaporization and cracking of liquid oil injected in a gas–solid riser*. Chemical Engineering Science, 2005. **60**(22): p. 6049-6066.
4. Patel, R., et al., *Effect of injection zone cracking on fluid catalytic cracking*. AIChE Journal, 2013. **59**(4): p. 1226-1235.
5. Huang, Z. and T.C. Ho, *Effect of thermolysis on resid droplet vaporization in fluid catalytic cracking*. Chemical Engineering Journal, 2003. **91**(1): p. 45-58.
6. Bruhns, S. and J. Werther, *An investigation of the mechanism of liquid injection into fluidized beds*. AIChE Journal, 2005. **51**(3): p. 766-775.

7. Knapper Brian, A., et al., *Measurement of Efficiency of Distribution of Liquid Feed in a Gas-Solid Fluidized Bed Reactor*, in *International Journal of Chemical Reactor Engineering*2003.
8. Gu, W., K. Tuzla, and J.C. Chen, *Measurement of liquid spray evaporation in fast fluidized beds*1996. Medium: X; Size: pp. 153-154.
9. Lappas, A.A., et al., *Feedstock and catalyst effects in fluid catalytic cracking – Comparative yields in bench scale and pilot plant reactors*. *Chemical Engineering Journal*, 2015. **278**: p. 140-149.
10. Bollas, G.M., et al., *Five-lump kinetic model with selective catalyst deactivation for the prediction of the product selectivity in the fluid catalytic cracking process*. *Catalysis Today*, 2007. **127**(1–4): p. 31-43.
11. Gao, J., et al., *Simulations of gas-liquid-solid 3-phase flow and reaction in FCC riser reactors*. *AIChE Journal*, 2001. **47**(3): p. 677-692.
12. Chang, S.L. and C.Q. Zhou, *Simulation of FCC riser flow with multiphase heat transfer and cracking reactions*. *Computational Mechanics*, 2003. **31**(6): p. 519-532.
13. Chang, J., et al., *Computational investigation of hydrodynamics and cracking reaction in a heavy oil riser reactor*. *Particuology*, 2012. **10**(2): p. 184-195.
14. Behjat, Y., S. Shahhosseini, and M.A. Marvast, *Simulation study of droplet vaporization effects on gas–solid fluidized bed*. *Journal of the Taiwan Institute of Chemical Engineers*, 2011. **42**(3): p. 419-427.
15. Gac, J.M. and L. Gradoń, *Lattice-Boltzmann modeling of collisions between droplets and particles*. *Colloids and Surfaces A: Physicochemical and Engineering Aspects*, 2014. **441**(0): p. 831-836.
16. Ge, Y. and L.-S. Fan, *Droplet–particle collision mechanics with film-boiling evaporation*. *Journal of Fluid Mechanics*, 2007. **573**: p. 311-337.
17. Mitra, S., et al., *Droplet impact dynamics on a spherical particle*. *Chemical Engineering Science*, 2013. **100**(0): p. 105-119.
18. Ardekani, A.M., S. Dabiri, and R.H. Rangel, *Deformation of a droplet in a particulate shear flow*. *Physics of Fluids (1994-present)*, 2009. **21**(9): p. 093302.
19. *FLUENT 14.5. Theory Guide*, 2011.
20. Sazhin, S.S., *Advanced models of fuel droplet heating and evaporation*. *Progress in Energy and Combustion Science*, 2006. **32**(2): p. 162-214.
21. Gianetto, A., et al., *Fluid Catalytic Cracking Catalyst for Reformulated Gasolines. Kinetic Modeling*. *Industrial & Engineering Chemistry Research*, 1994. **33**(12): p. 3053-3062.
22. Yaws, C.L., *Thermophysical Properties of Chemicals and Hydrocarbons*2014: Elsevier Science.
23. Yaws, C.L., *Transport Properties of Chemicals and Hydrocarbons*2014: Elsevier Science.
24. Yaws, C.L., P.K. Narasimhan, and C. Gabbula, *Yaws' Handbook of Antoine Coefficients for Vapor Pressure (2nd Electronic Edition)*, Knovel.
25. Sadeghbeigi, R., *Fluid Catalytic Cracking Handbook: An Expert Guide to the Practical Operation, Design, and Optimization of FCC Units*2012: Butterworth-Heinemann.
26. Mahulkar, A.V., G.B. Marin, and G.J. Heynderickx, *Droplet–wall interaction upon impingement of heavy hydrocarbon droplets on a heated wall*. *Chemical Engineering Science*, 2015. **130**: p. 275-289.
27. Nikolopoulos, N., A. Theodorakakos, and G. Bergeles, *Three-dimensional numerical investigation of a droplet impinging normally onto a wall film*. *Journal of Computational Physics*, 2007. **225**(1): p. 322-341.